Available online at www.sciencedirect.com
SCIENCE DIRECT®
Journal of Magnetic Resonance 171 (2004) 124–130
JMR Journal of Magnetic Resonance
www.elsevier.com/locate/jmr

Velocity distributions remotely measured with a single-sided NMR sensor

F. Casanova, J. Perlo, B. Blümich*

Institut für Technische und Makromolekulare Chemie, RWTH Aachen, D-52056, Germany

Received 9 March 2004; revised 28 July 2004
Available online 11 September 2004

Abstract

The pulsed field gradient nuclear magnetic resonance (PFG NMR) method has proved to be a powerful non-invasive technique to measure molecular displacement in various systems. It has been largely implemented with conventional NMR magnets where the volume for housing the flow setup is restricted. In this work we present the first approach to measure velocity distributions ex situ implementing a pulsed field gradient sequence on a single-sided NMR sensor. The open geometry of these sensors provides access to NMR measurements of a large number of applications previously excluded by the geometry of conventional closed magnets. Both, the distortions to the displacement encoding observed when implementing a PFG sequence in the presence of strongly inhomogeneous B_0 and B_1 fields, and the performance of the modifications proposed to eliminate these distortions are shown by means of numerical simulations. An alternating stimulated spin-echo PFG sequence implemented to remotely measure velocity distributions was combined with a multi-echo acquisition scheme to significantly increase the sensitivity of the method. The technique was implemented to measure the velocity propagator in a fluid undergoing laminar flow and good agreement with the theoretical result is observed.

Keywords: Unilateral NMR; Mobile probes; Displacement encoding; Transport

1. Introduction

Pulsed-field-gradient nuclear magnetic resonance (PFG NMR) has proved to be a powerful tool to characterize molecular motion non-invasively [1,2]. The method is suited to study displacement in a wide range of time and length scales. For opaque materials, for which optical methods are excluded, there are few experimental methods able to determine molecular displacements in any detail. PFG NMR offers a number of advantages compared to other techniques [3], and has been widely used in biology, medicine, and material science. It has enabled, for example, the measurement of vascular flow in stems and petioles at various stages of plant development, as well as vascular blood flow at various stages in the cardiac cycle. Also numerous applications in porous media such as natural sandstones have helped to elucidate models that describe the transport of fluids within the porous structure [4]. Combined with high-resolution imaging methods, it is a unique experimental method to check numerical solutions to the Navier–Stokes equation for Newtonian liquids, or to validate constitutive equations used to describe the complex rheological behavior of non-Newtonian fluids [5,6]. In contrast to other methods it is not distorted by the vicinity of walls offering, for example, the possibility to study effects such as the wall slip observed in the velocity shear of polymer melts and solutions [7].

* Corresponding author. Fax: +49 241 8022185.
E-mail address: bluemich@mc.rwth-aachen.de (B. Blümich).

1090-7807/$ - see front matter © 2004 Elsevier Inc. All rights reserved.
doi:10.1016/j.jmr.2004.08.008

A number of PFG sequences has been implemented and tested in the homogeneous field of conventional superconducting and electro magnets. These magnets offer limited space to fit the flow setup, restricting the application field of this technique. During the last years the interest has grown to develop open sensors for ex situ experiments [8–12]. These sensors select a volume inside objects of arbitrary size where the NMR measurement is performed. The versatility of such a device gives NMR access to a large number of applications excluded up to now by the closed geometries of conventional magnets. Different tool geometries have been designed and optimized for application in material analysis and quality control [9,10], well logging [11,12], water reservoir studies [13], moisture detection in composites [14], and medical diagnostics [15,16]. Sample characterization for these applications has been carried out mainly by measuring relaxation times, but the arsenal of new methods implemented on these sensors is growing, so that for example, diffusion–relaxation correlation maps [17] and even 3D images can be obtained [18].

Several problems appear when implementing a PFG sequence in the extremely inhomogeneous fields of these sensors. First, depending on the sequence the strong static gradient G_0 of the main field (of the order of some Teslas per meter) can introduce significant signal attenuation due to molecular self-diffusion. Second, the presence of such a gradient gives rise to large resonance offsets, which in addition to the inhomogeneities of the rf field, define a flip angle distribution in the sample. This inefficiency to apply uniform plane rotations introduces severe distortions in velocity measurements. Third, the low field (~10 MHz) and the broadband signal inherent to these sensors lead to low sensitivity that extends the experimental times to unviable limits.

In this work a modification to the PFG stimulated spin echo (STE) of Tanner [19], the so-called 13-interval sequence proposed by Cotts [20], was implemented to reduce the signal loss due to diffusion in the presence of the background gradient. In the next section the evolution of the magnetization during this sequence is studied in detail by means of numerical simulations, and a proper phase cycle to remove distortions coming from the flip angle distribution is described. Finally, to improve the signal-to-noise ratio a novel multi-echo acquisition scheme was implemented. Adding the echoes generated in the train a reduction in the experimental time up to two orders of magnitude was achieved.

The experiments were performed on a single-sided sensor equipped with both an optimized U-shaped magnet and a suitable gradient coil system described elsewhere [18]. To illustrate the performance of the technique, the velocity distribution of water undergoing laminar flow in a rectangular pipe was measured. The comparison with the theoretical propagator calculated for this geometry shows excellent agreement with the experimental results.

2. Method

2.1. PFG-STE in homogeneous B_0 and B_1 fields

PFG methods measure coherent and diffusive displacement by means of spin echoes (SE) [21] and stimulated echoes [19] formed in the presence of pulsed field gradients. In systems where T_2 is much shorter than T_1, the PFG-STE sequence of Tanner has been demonstrated to be better suited than the conventional PFG-SE sequence. PFG-STE enhances the length of the evolution interval between the encoding and decoding gradient pulses (Fig. 1A) by storing the phase information in the longitudinal magnetization. In this way the relaxation rate during Δ is given by T_1 and not by T_2 as in the SE sequence.

Fig. 1A shows Tanner's sequence, where a pair of gradient pulses of length δ introduces phases ϕ_i and ϕ_f proportional to the initial and final positions r_i and r_f [19]. The first gradient pulse completely spreads the magnetization in the transverse plane. When the second rf pulse is applied only half of the transverse magnetization is stored in the longitudinal direction, whereas the other half remains on the plane and is destroyed by homo-spoil gradients. Usually this is considered to be

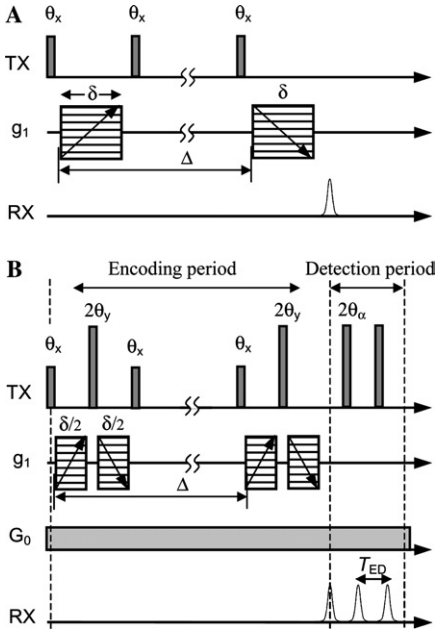

Fig. 1. (A) Stimulated spin-echo PFG sequence to measure displacement during the free evolution period Δ. (B) 13-interval PFG-STE sequence (*encoding period*) used to cancel the effect of the strong static gradient generated by the open magnet geometry. Refocusing 2θ pulses are applied during the coding intervals to cancel the phase spread due to the static gradient. To increase the sensitivity a train of rf pulses (*detection period*) is applied after the formation of the stimulated echo. The echo time T_{ED} for detection is determined by the dead time of the probe.

just a loss in sensitivity, but by loosing this magnetization component one can no longer distinguish the sign of the encoding gradient pulse. For this reason the stimulated echo has two contributions, one is modulated by a phase $(\phi_f - \phi_i)$ proportional to the displacement, and the second one by a phase $(\phi_f + \phi_i)$, proportional to the position [22]. When the response is sampled both contributions are present obtaining the superposition of the velocity distribution and the image of the sample.

To show this distortion, the evolution of the magnetization was calculated for the pulse sequence of Fig. 1A. For these simulations a homogeneous static magnetic field B_0 along the z-axis, a homogeneous rf field B_1 along y-axis, a pulsed field with a constant gradient g_1 along the x-axis, and non-interacting spins were assumed. For the sake of simplicity, a single velocity component of 20 mm/s inside a slice 2 mm thick and perpendicular to the velocity direction was considered. The q space [1] was sampled by stepping the gradient amplitude g_1 from positive to negative values.

Fig. 2A shows the profile obtained by Fourier transformation, where not only the peak at 20 mm/s but also a hat function between −20 and 0 mm/s are observed. The hat function is the image of the slice whose position can be observed on the space axis on top of the plot. The association of each contribution with the terms modulated by the phases $(\phi_f - \phi_i)$ and $(\phi_f + \phi_i)$ is straightforward. To cancel the contribution of the term proportional to the average position, the phases of the second and third rf pulses from x to y, and the receiver phase from x to $-x$. By adding both experiments the sign of the first gradient pulse is recovered and the unwanted image is complete removed (Fig. 2B). In the presence of inhomogeneities in the static magnetic field, the phases ϕ_i and ϕ_f are defined by the superposition of both the pulsed and the static gradient. If the static gradient is strong enough to define a T_2^* shorter than the encoding time δ, the term modulated by the phase $(\phi_f + \phi_i)$ will be averaged to zero even in absence of the pulsed gradient and will not contribute to the stimulated echo.

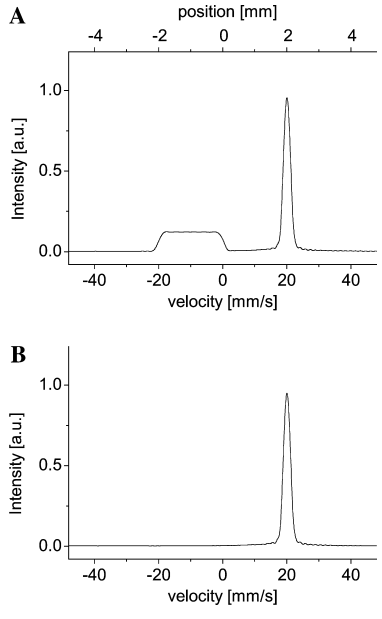

Fig. 2. (A) Simulated velocity profile for the PFG-STE sequence (Fig. 1A). A single velocity of 20 mm/s inside a slice 2 mm thick and perpendicular to the flow direction was assumed. Not only a single velocity is obtained, but also the image of the slice is observed. (B) The unwanted image is completely remove by cycling the phases of the second and third rf pulses between x and y.

2.2. PFG-STE in inhomogeneous B_0 and B_1 fields

When a static magnetic field gradient G_0 is present during the experiment, the signal obtained with the conventional PFG-STE sequence suffers from additional diffusion attenuation, which is proportional to G_0^2 and to a cross-term of the pulsed gradient g_1 and G_0 [20,23]. This complicates and in some cases prevents the use of this method for displacement encoding. The 13-interval sequence denoted as *encoding period* in Fig. 1B has been developed to reduce the diffusive signal attenuation due to G_0 [20]. It includes π pulses applied during the coding intervals to cancel the phase introduced by G_0 during this period, while the encoding phase is defined by means of bipolar gradient pulses to restore the effective gradient pulse length δ. In contrast to the PFG-SSE sequence, the additional diffusive attenuation due to G_0 arises only during the two encoding periods, but not during Δ. The sequence has been widely applied to measure flow in heterogeneous samples such as porous media showing that distortions introduced by field inhomogeneities can be reduced considerably. It must be noticed that as the sequence refocuses the phase introduced by the static gradient, the term modulated by the phase $(\phi_f + \phi_i)$, which is averaged out in the case of a STE sequence, is recovered. For this reason a phase cycle to eliminate the image from the velocity profile is needed. In the case of the 13-interval sequence, the phases of the third and fourth pulses are cycled from x to y, keeping the receiver phase constant.

Unfortunately, the implementation of this sequence in an open sensor, where the B_0 and B_1 fields are strongly inhomogeneous is not straightforward. The effective flip angle θ defined by an rf pulse depends on the amplitude B_1 of the rf field, the pulse length t_p, and the off-resonance field B_{off}. As a consequence of the space dependence of both B_{off} and B_1 a complex distribution of flip angles is obtained. It generates a large number of coherence pathways most of them being unfavorably encoded by the pulsed gradients.

To understand the performance of the pulse sequence, the signal response was calculated as a function of the effective flip angle assuming a single velocity v.

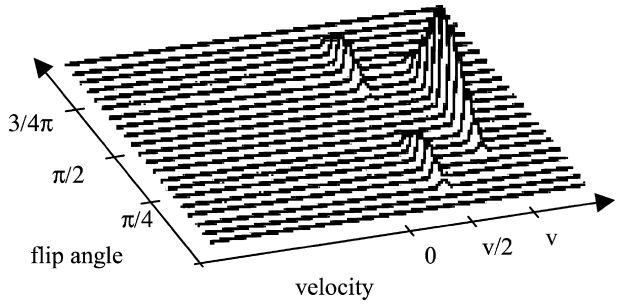

Fig. 3. Velocity profiles obtained as a function of the flip angle. For the calculation homogeneous static and rf fields were assumed as well as a uniform velocity v. A correct velocity distribution is obtained for flip angles close to $\pi/2$, whereas the profiles become completely distorted for flip angles close to $\pi/4$ and $3\pi/4$.

Fig. 3 shows the velocity distribution obtained as a function of the flip angle. For θ values close to the ideal value of $\pi/2$ the profile is undistorted and the single velocity is at the right spectral position. Nevertheless, when θ deviates from the ideal value (either because of B_1 or B_{off} variations), a spurious contribution at half of the original velocity value is obtained. This peak corresponds to the magnetization encoded by only one of the two gradient pulses during each coding period, which is modulated with half of the correct frequency in q space. This result shows, that although distortions appear for improper flip angles, they only contribute to signal at the half of the correct velocity value.

To quantify the importance of this distortion for the conditions of a real experiment we included in the calculations the off-resonance excitation and the real B_1 distribution of the rf coil. Fig. 4A shows the obtained velocity distribution. The peak at $v/2$ is clearly observed and its relative intensity is almost 50% compared to the intensity at the correct velocity. As can be observed in Fig. 3, the distortion is largest for flip angles close to $\pi/4$. For this value a large component of the magnetization remains along the z-axis after the application of the first rf pulse and is not encoded by the first gradient pulse of the encoding period. This remnant component is eliminated by cycling the phase of the first rf pulse and the phase of the receiver from x to $-x$ (add-subtract phase cycling). Fig. 4B shows the velocity profile obtained by including this phase cycle in the simulation. The distortion is now absent.

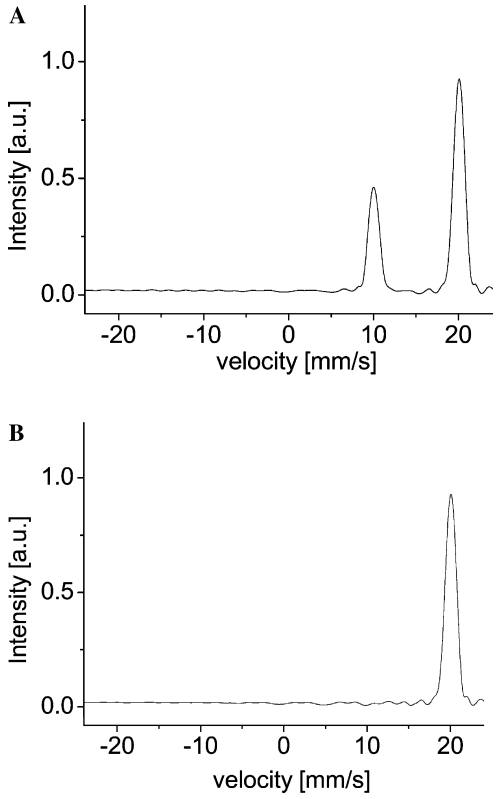

Fig. 4. (A) Velocity profile calculated considering both the off-resonance due to the static gradient of the sensor and the B_1 field distribution provided by the rf coil. Although a single velocity of 20 mm/s was assumed in the simulation, a contribution at half of this value is observed. (B) To effectively cancel this distortion, the phase of the first rf pulse and the receiver phase were cycled from x to $-x$.

2.3. Sensitivity improvement

Besides the mentioned distortions that appear as a consequence of the field inhomogeneity, an important limitation to the implementation of this technique is imposed by the poor sensitivity of single-sided sensors. In a previous work we have presented a multi-echo acquisition scheme, which, when applied after the encoding period of an imaging sequence, allowed us to improve the sensitivity up to one order of magnitude by adding the echoes in the train [18]. Based on the same concept a train of refocusing pulses denoted as *detection period* in Fig. 1B was attached to the 13-interval sequence (*encoding period*). As described in our previous work, the refocusing pulses only preserve the component of the echo signal parallel to the rf field, while the perpendicular component goes to zero after a transient period. For the reconstruction of the velocity distribution both magnetization components are necessary, and the loss of one of them mirrors the spectrum. To sample both components two experiments are performed, switching the phase of the rf pulses of the refocusing train from x to y. The full complex signal is then obtained by combining the x component of the first train with the y component of the second one.

In summary, the total experiment requires a minimum of eight scans per gradient step. The phase of the first rf pulse must be cycled from x to $-x$ to eliminate distortions due to the flip angle distribution, the phase of the third and fourth rf pulses from x to y to eliminate the unwanted image from the velocity profile, and the

sequence must be repeated changing the phase of the refocusing train to sample both components of the echo signal.

3. Experiments and results

A U-shaped magnet with an optimized field profile was used to provide the static magnetic field. Due to the strong magnetic field gradient along the depth direction different slices perpendicular to this direction can be precisely selected by adjusting the transmitter frequency [18]. For excitation and detection of the NMR signal, a 40 mm squared coil was used. The coil geometry combined with the depth selection defines a flat sensitive volume 36×26 mm^2 wide and 1 mm thick. When the slice is localized at 10 mm above the sensor surface the frequency is about 8 MHz, and the static gradient is 2.5 T/m. The sensor is equipped with a gradient coil system positioned underneath the rf coil that provides pulsed gradients along the two lateral dimensions. The maximum pulsed gradient available at the surface of the sensor is 20 mT/m. The total sensor size, which is determined by the magnet size, is 30×30 cm^2 along the lateral direction and 15 cm in height.

The efficiency of the sequence of Fig. 1B to remove the background gradient was tested first. The sequence was implemented without gradient pulses, and the echo intensity from water doped with Cu_2S was sampled as a function of Δ for different δ values. The acquired decays could be fitted by a mono-exponential function with a time constant independent of δ and equal to T_1 in all cases. This result proves that the stimulated echo stored as longitudinal magnetization during Δ is free of phase contributions introduced by the static gradient.

To illustrate the performance of the method, the water flow in a thin rectangular pipe was measured. The tube, 12 mm wide, 0.6 mm high, and 200 mm long, was placed at 10 mm from the sensor surface. When the ratio between the height a and the width b of the tube is $b/a \gg 1$, the velocity profile of laminar flow can be considered to be flat along the long side b while it changes as a quadratic function of the height a [24]. A volume flow rate Q of 170 ml/h was driven by a precision pump Pharmacia P500 defining a maximum velocity $v_m = 3/2 \times Q/(ab)$ of about 10 mm/s. The doted velocity profile in Fig. 5 was obtained with the sequence of Fig. 1B. The q space was sampled in 24 steps from negative to positive values and with the field of flow set to 30 mm/s a velocity resolution of about 1.25 mm/s was defined. To excite all the spins across the tube, the length of rf pulses was set to 7 μs defining a slice thickness of about 1 mm. The shortest echo time $T_{ED} = 0.11$ ms, limited by the dead time of the probe, was employed. A train of 2000 echoes was added to improve the sensitivity by a factor of 20 compared to single-echo detection. Thanks to this dramatic sensitivity enhancement, only 8 scans were required, determining a total time of about 5 min to measure the velocity distribution. The theoretical velocity profile for this pipe geometry was calculated and is shown in Fig. 5 as well. The good agreement between experimental and theoretical curves proves that the method is suitable to remotely measure velocity distributions, even in these extremely inhomogeneous fields.

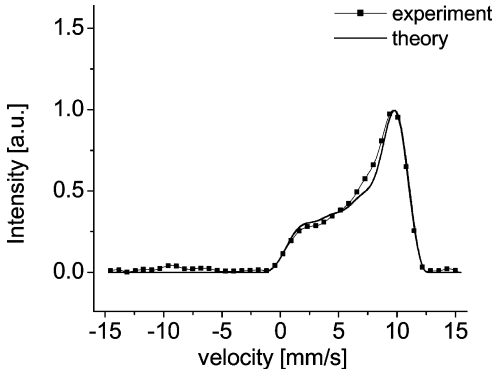

Fig. 5. Velocity distribution of water flowing in a rectangular pipe measured with the pulse sequence of Fig. 1B. Dots denote experimental data. The water used for the experiment was doped with Cu_2S to reduce the T_1 value to 0.9 s. The gradient pulse length δ was set to 0.5 ms and the evolution period Δ to 200 ms. To improve the signal-to-noise ratio 2000 echoes were acquired with $T_{ED} = 0.11$ ms. The total experimental time to obtain the velocity distribution working at 10 mm from the sensor surface was 5 min. For comparison the theoretical distribution was calculated and is shown as a continuous line.

Single-sided sensors are usually repositioned to scan the object at different spots. In some applications only the average velocity at each spot is required. When this is the case a single phase-encoding step can be used instead of the N steps needed to reconstruct the full propagator [25]. The sacrifice in velocity resolution leads to a direct reduction in experimental time by a factor of $N/2$. The procedure requires an initial experiment without gradient pulses to measure the reference phase of the echo signal, and a second experiment with the gradient

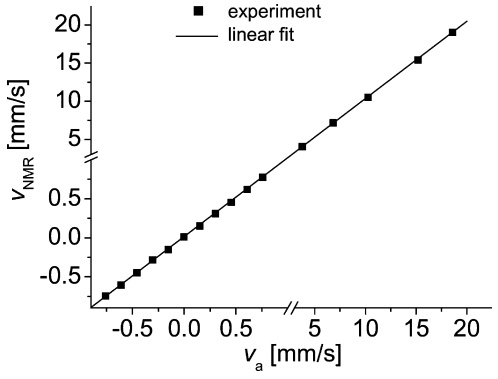

Fig. 6. Correlation between the average velocity v_{NMR} measured using the single-step phase encoding PFG-STE method with the value v_a, determined from the known flow rate and the geometry of the tube.

pulses to introduce a phase shift in the echo proportional to the displacement. From this phase shift the average velocity inside the sensitive spot can be easily computed. The method was implemented to measure the average velocity $v_a = Q/(ab)$ in the rectangular pipe. Fig. 6 shows the average velocity v_{NMR} measured with the single-step PFG-STE method as a function of the average velocity calculated via the known flow rate. The excellent correlation observed shows that the method is accurate in a wide velocity range. The time to measure the average velocity inside the selected volume, under the same conditions as in the previous experiment, was about 24 s.

4. Conclusion

The detailed information about fluid transport properties provided non-invasively by NMR, together with the simplicity of the measurement procedure identifies NMR as a suitable technique to characterize processes where flow conditions of complex fluids need to be known. In this work an alternated PFG-STE sequence suitable to encode displacement in the presence of strong B_0 and B_1 field gradients has been presented. It has successfully been implemented on a single-sided NMR sensor to measure velocity distributions ex situ. One of the key points to develop this approach to a method of practical use was the incorporation of a multi-echo acquisition scheme following the displacement encoding period. Adding the large number of echoes collected for liquid samples, a dramatic reduction in the experimental time was achieved so that velocity distributions can be measured in a few minutes. The time reduction that can be obtained in this way is determined by the number of echoes acquired in the generated echo train. In the presence of a 2.5 T/m static gradient and for liquids with long T_2 the time decay is determined by the diffusion coefficient. While for water 2000 echoes were acquired, the number would be considerably larger for more viscous samples like oil. The short experimental time needed to explore the signal at a given depth suggest considering the implementation of two-dimensional experiments. Taking advantage of the depth selection that can be achieved by retuning the probe frequency we are currently engaged in obtaining spatially resolved velocity profiles. It is anticipated that the new unilateral flow sensor will find applications in non-invasive measurements of fluid transport in non-transparent media. Fluids of interest are molten polymers, polymers in solution, and a great variety of slurries, colloidal dispersions, fermentation products, foams, and a host of non-Newtonian liquids. These fluids have non-linear viscoelastic properties and the lack of models underlines the need of experimental techniques to measure the flow distribution.

Acknowledgment

FC thanks the Alexander von Humboldt Foundation for a research fellowship. Support of this project by the DFG Forschergruppe FOR333 ‘‘Surface NMR of Elastomers and Biological Tissue’’ is gratefully acknowledged.

References

[1] P.T. Callaghan, Principles of Nuclear Magnetic Resonance Microscopy, Clarendon Press, Oxford, 1991.
[2] B. Blümich, NMR Imaging of Materials, Clarendon Press, Oxford, 2000.
[3] Y. Xia, P.T. Callaghan, K.R. Jeffrey, Imaging velocity profiles: flow through an abrupt contraction and expansion, A.I.Ch.E.J. 38 (1992) 1408–1420.
[4] K.J. Packer, J. Tessier, The characterization of fluid transport in a porous solid by pulsed gradient stimulated echo NMR, Mol. Phys. 87 (1996) 267–272.
[5] Y.L. Yeow, J.W. Taylor, Obtaining the shear rate profile of steady laminar tube flow of Newtonian and non-Newtonian fluids from nuclear magnetic resonance imaging and laser Doppler velocimetry data, J. Rheol. 46 (2002) 351–365.
[6] D.F. Arola, R.L. Powell, G.A. Barrall, M.J. McCarthy, Pointwise observations for rheological characterization using nuclear magnetic resonance imaging, J. Rheol. 43 (1999) 9–30.
[7] Y. Xia, P.T. Callaghan, Study of shear thinning in high polymer solution using dynamic NMR microscopy, Macromolecules 24 (1991) 4777–4786.
[8] R.L. Kleinberg, A. Sezginer, D.D. Griffin, M. Fukuhara, Novel NMR apparatus for investigating an external sample, J. Magn. Reson. 97 (1992) 466–485.
[9] G. Eidmann, R. Salvelsberg, P. Blümler, B. Blümich, The NMR-MOUSE, A mobile universal surface explorer, J. Magn. Reson. A 122 (1996) 104–109.
[10] G.A. Matzkanin, A review of non-destructive characterization of composites using NMR, in: Non-destructive Characterization of Materials, Springer, Berlin, 1998, pp. 655.
[11] R.L. Kleinberg, Well logging, in: D.M. Grant, R.K. Harris (Eds.), Encyclopedia of NMR, Wiley, New York, 1996, pp. 4960–4969.
[12] J.A. Jackson, L.J. Burnett, F. Harmon, Remote (Inside-Out) NMR. III. Detection of nuclear magnetic resonance in a remotely produced region of homogeneous magnetic field, J. Magn. Reson. 41 (1980) 411–421.
[13] O.A. Shushakov, Ground water NMR in conductive water, Geophysics 61 (1996) 998–1006.
[14] P.J. Prado, NMR hand-held moisture sensor, Magn. Reson. Imag. 19 (2001) 505–508.
[15] US Patent 5,959,454. Bruker Analytic. Magnet arrangement for an NMR tomography system, in particular for skin and surface examinations.
[16] R. Haken, B. Blümich, Anisotropy in tendon investigated in vivo by a portable NMR scanner, the NMR-MOUSE, J. Magn. Reson. 144 (2000) 195–199.
[17] M.D. Hürlimann, M. Flaum, L. Venkataramanan, C. Flaum, R. Freedman, G.J. Hirasaki, Diffusion–relaxation distribution functions of sedimentary rocks in different saturation states, Magn. Reson. Imag. 21 (2003) 305–510.
[18] J. Perlo, F. Casanova, B. Blümich, 3D imaging with a single-sided sensor: an open tomograph, J. Magn. Reson. 166 (2004) 228–235.
[19] J.E. Tanner, Use of the stimulated echo in NMR diffusion studies, J. Chem. Phys. 52 (1970) 2523–2526.

[20] R.M. Cotts, M.J.R. Hoch, T. Sun, J.T. Markert, Pulsed field gradient stimulated echo methods for improved NMR diffusion measurements in heterogeneous systems, J. Magn. Reson. 83 (1989) 252–266.
[21] E.O. Stejkal, J.E. Tanner, Spin diffusion measurements: spin echoes in the presence of a time-dependent field gradient, J. Chem. Phys. 42 (1965) 288–291.
[22] R. Kimmich, NMR Tomography, Diffusometry, Relaxometry, Springer, Berlin, 1997, pp. 11–14.
[23] P.Z. Sun, J.G. Seland, D. Cory, Background gradient suppression in pulsed gradient stimulated echo measurements, J. Magn. Reson. 161 (2003) 168–173.
[24] P. Grondret, N. Rakotomalala, M. Rabaud, D. Salin, P. Watzky, Viscous parallel flows in finite aspect ratio Hele-Shaw cell: analytical and numerical results, Phys. Fluids 9 (1997) 1841–1843.
[25] Y. Xia, P.T. Callaghan, One-Shot velocity microscopy: NMR imaging of motion using a single phase-encoding step, Magn. Reson. Med. 23 (1992) 138–153.